Anisotropic properties of TaS_2

2007 Chinese Phys. 16 3809

(http://iopscience.iop.org/1009-1963/16/12/042)

Vol 16 No 12, December 2007
1009-1963/2007/16(12)/3809-06

Chinese Physics

Anisotropic properties of TaS_2*

Qiao Yan-Bin(乔彦彬)[a], Li Yan-Ling(李延龄)[a,b], Zhong Guo-Hua(钟国华)[a], Zeng Zhi(曾 雉)[a]†, and Qin Xiao-Ying(秦晓英)[a]

[a] *Key Laboratory of Materials Physics, Institute of Solid State Physics, Chinese Academy of Sciences, Hefei* 230031, *China*

[b] *Department of Physics, Xuzhou Normal University, Xuzhou* 221116, *China*

(Received 2 January 2007; revised manuscript received 17 May 2007)

The anisotropic properties of 1T- and 2H-TaS_2 are investigated by the density functional theory within the framework of full-potential linearized augmented plane wave method. The band structures of 1T- and 2H-TaS_2 exhibit anisotropic properties and the calculated electronic specific-heat coefficient γ of 2H-TaS_2 accords well with the existing experimental value. The anisotropic frequency-dependent dielectric functions including the effect of the Drude term are analysed, where the $\varepsilon^{xx}(\omega)$ spectra corresponding to the electric field $\boldsymbol{E}$ perpendicular to the z axis show excellent agreement with the measured results except for the $\varepsilon_1^{xx}(\omega)$ of 1T-TaS_2 below the energy level of 2.6 eV which is due to the lack of the enough CDW information for reference in our calculation. Furthermore, based on the values of optical effective mass ratio P of 1T and 2H phases it is found that the anisotropy in 2H-TaS_2 is stronger than that in 1T-TaS_2.

Keywords: anisotropic property, band structure, dielectric function
PACC: 7125, 7127, 7145Gm

1. Introduction

Transition-metal dichalcogenides compounds (TMDCs) have been of widespread interest for a long time because of their unique structural and electronic properties.[1,2] 1T- and 2H-TaS_2 are two prototypes for such materials. In the terms of structure, 1T and 2H phases can be regarded as strongly bonded two-dimensional S-Ta-S layers or sandwiches which are loosely coupled with each other by relatively weak Van der Waals forces. Within a single S-Ta-S sandwich, the Ta and S atoms form two-dimensional hexagonal arrays. The Ta atoms are octahedrally coordinated by six neighbouring S atoms in the 1T phase, whereas in the 2H phase, the coordination of Ta atoms is trigonal prismatic. 1T- and 2H-TaS_2 have rich phase diagrams of charge-density waves (CDWs). 1T-TaS_2 shows a $\sqrt{13}\times\sqrt{13}$ CDWs for $T < 540$ K which changes upon cooling from incommensurate to nearly commensurate at 350 K and then to commensurate at 180 K.[3] 2H-TaS_2 forms a 3×3 commensurate CDW states below 70 K[4] similar to those for 2H-$TaSe_2$.[5] Due to the weak Van der Waals interlayer forces, 1T- and 2H-TaS_2 can be intercalated and dramatically changed in their physical properties.[6,7] Recently, the experimental studies about TaS_2 have made great progress: it has obtained a continuous tuning of electronic correlations by alkali adsorption on layered 1T-TaS_2,[8] that is, there is a metal-insulator transition by changing the band-filling n, the on-site Coulomb correlation energy U, or the one-electron bandwidth W. The superconducting transition temperature (T_c) of 2H-TaS_2 has been enhanced by intercalating Na atoms (Na_xTaS_2).[9] It is found that the T_c rises with the increase of Na content.

Up to now, there have already existed electronic structure calculations for us to understand the 1T- and 2H-TaS_2. By applying the empirical tight-binding method to 1T- and 2H-TaS_2 in the presence of a commensurate CDW, Smith *et al*[10] have shown that in reconstruction in the presence of CDW phase the Ta d-band splits into three subbands with gaps in 1T-TaS_2, but the effect of CDW on the electronic structure is very weak in 2H-TaS_2. And the nonrelativistic augmented-plane-wave (APW) method was employed by Matthesis[11] to calculate the electronic band structures of 1T- and 2H-TaS_2 and metallic behaviour was predicted for these compounds. While Myron and Freeman[12] exhibited the full-Brillouin-zone Fermi surfaces of 1T-TaS_2 and 1T-$TaSe_2$ us-

*Project supported by the National Natural Science Foundation of China (Grant Nos 90503005 and 50472097), the State Key Development Program for Basic Research of China (Grant No 2005CB623603), Knowledge Innovation Program of Chinese Academy of Sciences, and Director Grants of Hefei Institutes of Physical Sciences.
†Corresponding author. E-mail: zzeng@theory.issp.ac.cn

ing the Korringa–Kohn–Rostoker (KKR) method in the muffin-tin approximation. Woolley and Wexler[13] also calculated the Fermi surface of 1T-TaS_2 by using the layer method within the muffin-tin approximation. Sharma *et al*[14] presented the anisotropic frequency-dependent dielectric functions for 1T and 2H phases of TaS_2 and $TaSe_2$ using the linear muffin-tin orbital method within the atomic sphere approximation, in which their results were still shown to be unsatisfactory at the spectrum peak position compared with the experimental results. Recently, Reshak and Auluck[15] carried out the calculations about the electronic and optical properties of these compounds using full-potential linearized augmented plane wave (FP-LAPW) method in which the exchange-correlation potential was treated within the local density approximation (LDA). They analysed the effect on the electronic and optical properties when S was replaced by Se. Blaha [16] also used the same method earlier to discuss the bonding mechanism as well as the electronic field gradients of 2H TaS_2.

However, the existing calculations are still insufficient due to lack of detailed comparison between 1T- and 2H-TaS_2 phases, in particular their anisotropic properties, and accurate methods. Therefore in this work, we intend to emphasize the anisotropic properties of TaS_2 and compare in detail 1T- and 2H phases by using a more accurate full-potential method. It is found that the calculated frequency-dependent dielectric functions are in excellent agreement with experimental results.

The remainder of this paper is organized as follows: In Section 2 we give a brief description of the computational method. In Section 3 the main results and discussion are presented. The brief conclusions are given in Section 4.

2. Computational method

The calculations in this work are performed with the FP-LAPW method which is implemented in the WIEN2k package in a scalar relativistic version.[17] The generalized gradient approximation (GGA)[18] is adopted for the exchange-correlation potential. The charge density, potential and wavefunctions are expanded in spherical harmonics with $l \leq 10$ inside the muffin-tin spheres whose radii are set to 2.32, 2.06 a.u. for Ta and S atoms, respectively. We employ $28 \times 28 \times 13$ special k meshes in the irreducible Brillouin-zone (IBZ) for 1T-TaS_2, and $36 \times 36 \times 8$ meshes for 2H-TaS_2, respectively, and let $RK_{\max} = 7.0$ and $G_{\max} = 14$, resulting in about 1865 and 2030 plane waves. In our calculations the 4f5s5p5d6s of Ta and 3s3p orbitals of S atoms are treated self-consistently. The calculation and the integration of density of states on the IBZ are carried out using the tetrahedron method.[19]

Table 1. The lattice constants of TaS_2 of 1T and 2H phase.

Compound	a/Å	c/Å	c/a	
1T-TaS_2	3.38	6.19	1.83	This work
	3.36	5.85	1.74	Exp.[11]
2H-TaS_2	3.342	12.54	3.75	This work
	3.316	12.07	3.64	Exp.[20]

In 1T-TaS_2 (space group P-3m1) the unit cell contains three atoms in which the Ta atom is at 1 c (0, 0, 0) and two S atoms at 2 d $\pm(\frac{1}{3}, \frac{2}{3}, z)$ sites where $z \sim 0.25$. The unit cell of 2H-TaS_2 (space group $P6_3/mmc$) contains six atoms, the two equivalent Ta atoms are at $2b$ $\pm(0, 0, \frac{1}{4})$ and four S atoms are at $4f$ $\pm(\frac{1}{3}, \frac{2}{3}, z)$, $\pm(\frac{1}{3}, \frac{2}{3}, \frac{1}{2}\text{-}z)$ sites where $z \sim \frac{1}{8}$. The optimized lattice constants of TaS_2 of 1T and 2H phases are listed in Table 1 together with their experimental values. The IBZ for 1T-TaS_2 is very similar to that for 2H phase as shown in Fig.1, where Γ, M, K, A, L, H represent the special symmetry points on the IBZ edge.

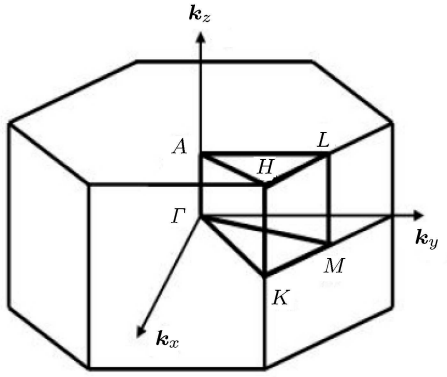

Fig.1. The Irreducible Brillouin Zone of TaS_2 of 1T and 2H phases.

3. Results and discussion

3.1. The feature of electronic bands

The calculated band structure for 1T-TaS_2 is shown in Fig.2(a). The bands are localized along Γ-M-K-Γ, A-L-H-A and Γ-A directions. S s-state is far away from the Fermi level around the energy

range from −15.2 to −15.5 eV. The bands ranging from −7.0 to −1.3 eV are mainly of S p-state and have a slight contribution from Ta d-state. The bands between −1.2 and 2.9 eV as well as between 3.4 and 6.0 eV are mainly of Ta d-state. The mixing of S p and Ta spd-states appears above 6.0 eV. The occupied Ta d-state below Fermi level exists only along *Γ*-*M*-*K* and *A*-*L*-*H* directions, and there is no occupied d-state along *K*-*Γ*-*A* and *H*-*A* directions. The bandwidth of occupied Ta d is about 1.33 eV which is in good agreement with the value 1.16 eV obtained from the results using the layer method[13] and also with the experimental value 1.5 eV through photoemission studies.[21] In particular, S p-states coincide with the measured results from the angular-resolved photoemission experiment,[22] which has a rigid shift by about 1.35 eV to wards the high energies compared with the APW results.[11] From this figure it is also found that the bands along the *Γ*-*M*-*K*-*Γ* and *A*-*L*-*H*-*A* directions are nearly identical near the Fermi level and very weakly dispersed along *Γ*-*A* direction, implying no significant interaction along the *z* direction. These two features of bands described above indicate that 1T-TaS_2 is a quasi-two-dimensional system.

Figure 2(b) illustrates the band structure of 2H-TaS_2. Here S s-state is also away from the Fermi level ranging from −14.4 to −12.0 eV. From −6.2 to −0.3 eV the bands are contributed from S p-state and a mixture with Ta d-state. The p-state in 2H phase shifts towards high energies by about 0.8 eV with respect to Fermi level compared with that in 1T phase. The bandwidth of S p band in 2H phase is 5.9 eV which is nearly the same as that in 1T phase and is very close to the experimental values $6.0 - 7.0$ eV.[21] Between −0.5 and 6.0 eV the bands mainly come from the Ta d-state. The bands above 6.0 eV are composed of S p and Ta spd-states. The crystal field in 2H phase resulting from trigonal prismatic coordination of Ta atoms by S atoms splits off a narrow subband which corresponds roughly to the Ta d_{z^2} subband, and the small energy gap is 0.5 eV which is in excellent agreement with Reshak's result[15] but is slightly less than the value 1.0 eV obtained by Matthesis.[11] The occupied Ta d subband below the Fermi level exists along *Γ*-*M*-*K*-*Γ* and *A*-*L*-*H*-*A* directions while it exists only along *Γ*-*M*-*K* and *A*-*L*-*H* directions in 1T phase. We also find that the bandwidth of the occupied Ta d-state is 0.5 eV which is smaller than that (1.33 eV) of 1T phase. In addition, the Ta d_{z^2} subband manifests a split along the *Γ*-*M*-*K*-*Γ*-*A* direction due to the interlayer d–d interactions.[22]

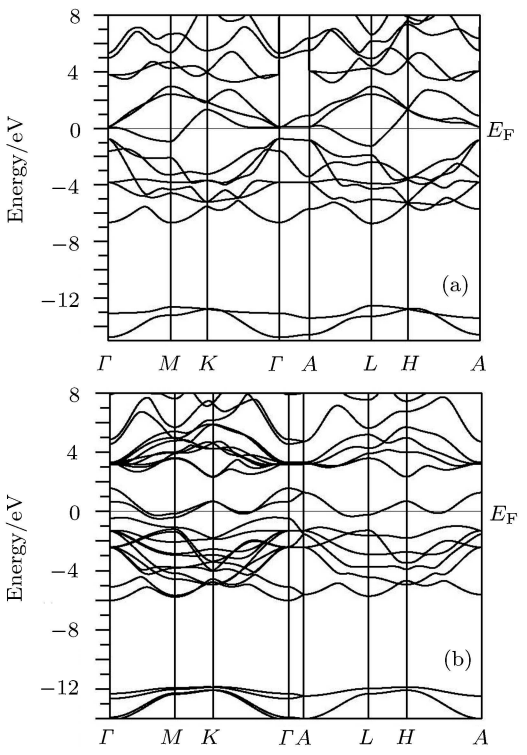

Fig.2. The band structures of (a) 1T-TaS_2, (b) 2H-TaS_2.

3.2. Decomposed density of states

The decomposed density of states of 1T-TaS_2 is shown in Fig.3(a). We notice that Ta d state splits into three lower t_{2g} (d_{z^2}, d_{yz}, $d_{x^2-y^2}$) and two degenerate upper e_g (d_{xy}, d_{yz}) because of the lattice distortion. The energy separation between t_{2g} and e_g is about 0.6 eV. A strong hybridization between S p and Ta d appears in valence and conduction bands ranging from −7.0 to 6.0 eV, which determines the transport properties of 1T-TaS_2. The states in this range consist of three main peaks that are assigned to pdπ and pdσ bondings ($-7.0 - 1.2$ eV), Ta t_{2g} antibonding ($-1.2 - 2.9$ eV) and e_g antibonding ($3.4 - 6.0$ eV). The value of the density of states at the Fermi level (N (E_F)) is 1.512 states/eV per unit cell as shown in Table 2. These data can give the electronic specific-heat coefficient γ of about 3.56 mJ/mol·K^2. However, we cannot find any experimental data about the electronic specific-heat coefficient of 1T-TaS_2 for reference.

Figure 3(b) presents the decomposed density of states of 2H-TaS_2. Owing to the trigonal prismatic

coordination of Ta atoms in 2H phase, there appears a dramatic change in decomposed density of states compared with that of 1T phase. The e_g subband shifts towards lower energies while the t_{2g} subband shifts to higher energies with respect to Fermi level, meanwhile, the band gap between t_{2g} and e_g disappears. In other words, Ta d state splits into upper subband (d_{xy}, d_{yz}, d_{xz}) and lower narrow subband (d_{z^2}, $d_{x^2-y^2}$). A strong hybridization between S 3p and Ta 5d appears in a range from −6.2 to 6 eV. The states in this range are assigned to pdπ and pdσ bondings (−6.2−0.5 eV), t_{2g} and e_g antibondings (−0.5−6.0 eV). The N (E_F) is 4.67 states/eV per unit cell (shown in Table 2) which is about 3.1 times that in 1T phase. This datum is consistent with the previous theoretical values 4.6−4.8 states/eV per unit cell.[11,15] and is also close to the experimental value 6.5 states/eV per unit cell.[23] And it leads to the electronic specific-heat coefficient γ of about 11.02 mJ/mol·K^2 which is comparable well with the experimental value of 8.5 mJ/mol·K^2,[24] implicating that the present description of the electronic property is quite acceptable.

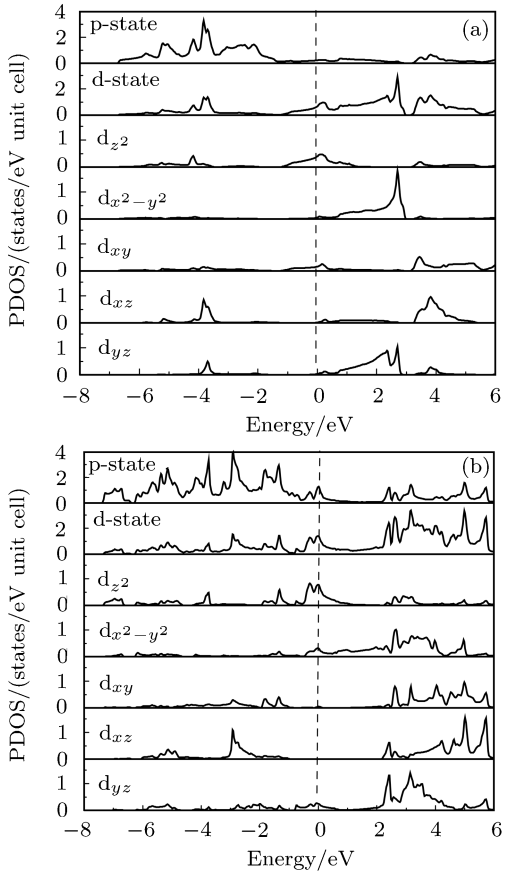

Fig.3. The decomposed density of states of (a) 1T-TaS_2, (b) 2H-TaS_2.

Table 2. The DOS at the Fermi level $N(E_F)$(States/eV per unit cell), electronic specific-heat coefficient γ(mJ/mol·K^2), the plasma frequency ω_P(eV) and the value m_{xx}/m_{zz}.

Compound	N (E_F)	γ	ω_P^{xx}	ω_P^{zz}	m_{xx}/m_{zz}
1T-TaS_2	1.512	3.56	5.415	1.59	0.09
2H-TaS_2	4.67	11.02	3.524	0.91	0.07

3.3. The frequency-dependent dielectric functions of 1T- and 2H-TaS_2

The frequency-dependent dielectric functions including the intraband contribution is $\varepsilon(\omega)=\varepsilon_1(\omega)+i\varepsilon_2(\omega)$, where $\varepsilon_1(\omega)$ and $\varepsilon_2(\omega)$ are the real and imaginary parts of the function, respectively. The $\varepsilon(\omega)$ is calculated within the random phase approximation (RPA) based on the calculated band structure. The imaginary part $\varepsilon_2(\omega)$ is calculated from the momentum elements between the occupied and unoccupied wavefunctions. The real part $\varepsilon_1(\omega)$ is obtained by means of Kramers–Kroning relation. In 1T- and 2H-TaS_2 the $\varepsilon^{xx}(\omega)$ and $\varepsilon^{zz}(\omega)$ correspond to the electric field $\boldsymbol{E}$ perpendicular and parallel to the z axis, respectively.

The dependences of $\varepsilon_2^{xx}(\omega)$ and $\varepsilon_2^{zz}(\omega)$ on photon energy in a range of 0–13.6 eV are shown in Figs.4(a)–(b), which demonstrate sizable anisotropies of 1T- and 2H-TaS_2. The $\varepsilon_2^{xx}(\omega)$ of 1T-TaS_2 is shown to be in good agreement with the measured data (see Fig.10(a) in Ref.[22]). Particularly the special features of our results accord very well with their corresponding experimental results: two maxima of $\varepsilon_2^{xx}(\omega) = 15.51$ at 1.1 eV and $\varepsilon_2^{xx}(\omega) = 10.79$ at 6.5 eV and a minimum of $\varepsilon_2^{xx}(\omega)$=3.19 at 3.17 eV in our calculation of Fig.4(a) correspond to the two maxima of $\varepsilon_2(\omega) = 24.6$ at 1.3 eV and $\varepsilon_2(\omega) = 12.2$ at 6.5 eV, and a minimum of $\varepsilon_2^{xx}(\omega) = 2.3$ at 3.7 eV in the measured results. Additionally, from this figure it is found that the contribution from the Drude term (intraband contribution)is significant for energies below 1.0 eV for 1T-TaS_2. The curve of $\varepsilon_2(\omega)$ reveals the critical points at around 1.1, 5.5, 6.5, 9.3, 10.3 eV which are assigned to $A_1 - A_5$ in turn. A_1 and A_2 peaks primarily originate from the transition of S p to Ta t_{2g} bands. And $A_3 - A_5$ peaks mainly come from the transition of S p to Ta e_g bands.

As for the case of 2H-TaS_2, the $\varepsilon_2^{xx}(\omega)$ spectrum (Fig.4(b)) is also comparable well with the measured data (see Fig.9(a) in Ref.[25]): a maximum of $\varepsilon_2^{xx}(\omega) = 10.8$ at 3.7 eV corresponding to the experimental data of 11.8 at 3.7 eV, a minimum of

$\varepsilon_2^{xx}(\omega) = 1.5$ at 1.5 eV corresponding to the experimental data of 1.2 at 1.9 eV, and another maximum of $\varepsilon_2^{xx}(\omega) = 12.8$ at 4.9 eV matching the experimental data of 11.5 at 5.0 eV. Obviously, the effect of the Drude term is significant for energies less than 0.2 eV. The dielectric function is highly anisotropic for the energies less than 10 eV. The critical points at around 1.0, 3.7, 4.9, 6.4, 7.1, 8.8 eV are assigned to $B_1 - B_6$ in turn. The structure B_1 is dominated by transition from S p to Ta d_{z^2} bands, and $B_2 - B_6$ peaks are due to the transitions of S p to the mixture of Ta t_{2g} and e_g bands.

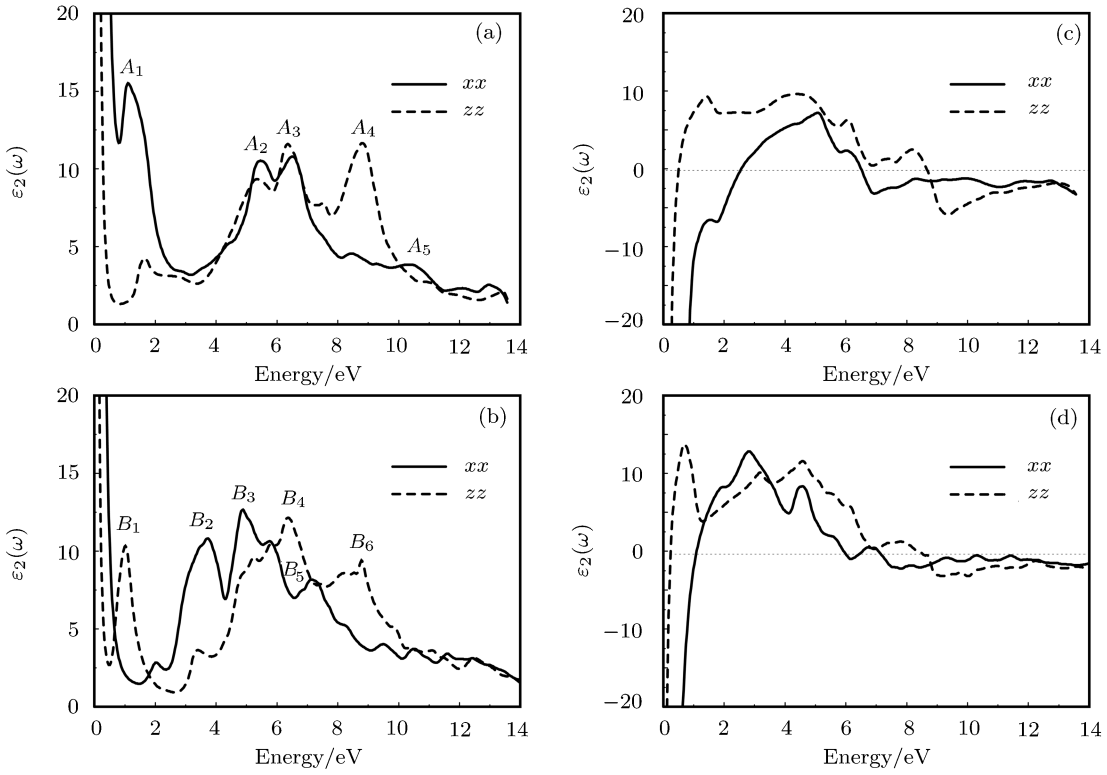

Fig.4. The frequency-dependent dielectric functions: the imaginary parts of (a) 1T-TaS_2, (b) 2H-TaS_2; the real parts (c) 1T-TaS_2, (d) 2H-TaS_2.

The real part of the dielectric function is derived from the imaginary part using Kramers-Kroning relation. The calculated $\varepsilon_1^{xx}(\omega)$ for 1T (Fig.4(c) primarily matches the experimental curve shown in Fig.10(a) of Ref.[23], and that of 2H-TaS_2 agrees well with the experimental results shown in Fig.9(a) of Ref.[22]. However, the calculated $\varepsilon_1^{xx}(\omega)$ of 1T-TaS_2 in the energies below 2.6 eV exhibits big difference from the experimental results of which the curve goes down to negative, presenting a semi-conductor behaviour. As mentioned above, the experiments confirmed the presence of nearly commensurate CDW phase which might lead to a narrow-bandgap semiconductor for 1T-TaS_2, while our present calculations are carried out without enough CDW information and consequently give out metallic ground state. Calculations including enough CDW information will be discussed elsewhere.

In the low energy range the effect of Drude term is very accountable. We can see from Figs.4(c)–(d) that there exists a very large static dielectric constant ($\varepsilon_1(\omega)$, $\omega = 0$), which means that in 1T and 2H phases the screening effect is very strong so that the electron-hole interactions in 1T and 2H phases are very weak, that is, the excitonic effect may be very weak. Both in 1T- and 2H-TaS_2 the values of $\varepsilon_1^{xx}(\omega)$ drop to negative values beyond 6.5 and 5.9 eV, respectively, which are comparable well with the experimental values 6.6 and 6.4 eV. The plasma frequency ω_P values are shown in Table 2. It is known that the plasma frequency describes the collective excitations within the long wavelength limit and $\omega_P^2 = 4\pi ne^2/m$,[26] where n is the electron concentration and m is the optical effective mass. Therefore, the optical effective mass is inversely proportional to the square of the plasma frequency so that we can obtain the ratio of anisotropy optical effective mass $P = m_{xx}/m_{zz} = (\omega_P^{zz}/\omega_P^{xx})^2$ in one

system where n is assumed to be a constant. The dimensionless P describes the strength of anisotropy of a system, and $P = 1$ indicate that the system is isotropic. We find that the P values are 0.09 and 0.07 for 1T- and 2H-TaS_2, respectively, which imply that TaS_2 is anisotropic both for 1T and 2H phases. We can also see the anisotropic feature from the band structure above. Simultaneously, the deviation from 1 of P value for 2H phase is much larger than that for 1T phase, which implicates that the anisotropy in 2H phase is stronger than that in 1T phase.

4. Conclusions

We have reported the anisotropic properties via the electronic structure and the frequency-dependent dielectric functions of TaS_2 of 1T and 2H phases without including the specific information of CDWs using the first-principles FP-LAPW method with the GGA exchange-correlation. A parallel comparison between 1T and 2H phases is made in detail. It is found that the S p and Ta d states dominate the valence and conduction bands of 1T- and 2H-TaS_2. The locations of S p and Ta d states with respect to the Fermi level, obtained from the present calculation, are in very good agreement with the experimental results. The densities of states at the Fermi level for 1T- and 2H-TaS_2 are 1.512 and 4.67 states/eV per unit cell, respectively, leading to the values of electronic specific-heat coefficient γ of 3.56 and 11.02 mJ/mol·K^2, respectively. The frequency-dependent dielectric functions present critical points of $A_1 - A_5$ and $B_1 - B_6$ in $\varepsilon_2(\omega)$ of 1T- and 2H-TaS_2, which are determined with respect to the energy transitions in band structure. The large static dielectric functions in 1T- and 2H-TaS_2 indicate that there exists a very strong screening effect, in other words, the excitonic effect is very weak in such systems. From the band structure feature as well as the optical effective mass ratio P we conclude that there exist anisotropic (two-dimensional characteristic) properties in 1T- and 2H-TaS_2 and the anisotropy in 2H phase is stronger than that in 1T phase. Most of the calculated properties are comparable well with the experimental results except for the $\varepsilon_1^{xx}(\omega)$ of 1T-TaS_2 below the energy level of 2.6 eV. We believe that the CDW phase plays an important role in that energy range.

Acknowledgment

Part of the calculations were performed at the Centre for Computational Science, Hefei Institute of Physics China.

References

[1] Zhou K J, Tezuka Y, Cui M Q, Ma C Y, Zhao Y D, Wu Z Y and Yagishita A 2007 *Acta Phys. Sin.* **56** 2986 (in Chinese)
[2] Zhang H, Wang B Y, Zhang R Q, Zhang Z, Qian H J, Su R, Kui R X and Wei L 2006 *Acta Phys. Sin.* **55** 2482 (in Chinese)
[3] Zwick F, Berger H, Vobornik I, Margaritondo G, Forró L, Beeli C, Onellion M, Panaccione G, Taleb-Ibrahimi A and Grioni M 1998 *Phys. Rev. Lett.* **81** 1058
[4] Thompson A H, Gamble F R and Koehler Jr R F 1972 *Phys. Rev.* B **5** 2811
[5] Moncton D E, Axe J D and DiSalvo F J 1975 *Phys. Rev. Lett.* **34** 734
[6] DiSalvo F J, Wilson J A, Bageley J G and Waszczak J V 1975 *Phys. Rev.* B **12** 2220.
[7] Bando H, Koizumi K, Miyahara Y and Ozaki H 2000 *J. Phys: Condens. Matter* **12** 4353
[8] Rossnagel K, Rotenberg E, Koh H, Smith N V and Kipp L 2005 *Phys. Rev. Lett.* **95** 126403
[9] Fang L, Wang Y, Zou P Y, Tang L, Xu Z, Chen H, Dong C, Shan L and Wen H H 2005 *Phys. Rev.* B **72** 014534
[10] Smith N V, Kevan S D and DiSalvo F J 1985 *J. Phys.* C **18** 3175
[11] Matthesis L F 1973 *Phys. Rev.* B **8** 3719
[12] Myron H W and Freeman A J 1974 *Phys. Rev.* B **11** 2735
[13] Woolley A M and Wexler G 1977 *J. Phys.* C **10** 2601
[14] Sharma S, Auluck S and Khan M A 2000 *Pramana J. Phys.* **54** 431
[15] Reshak A H and Auluck S 2005 *Physica* B **358** 158
[16] B Blaha P 1991 *J. Phys.: Condens. Matter* **3** 9381
[17] Blaha P, Schwarz K, Sorantin P and Trickey S B 1990 *Comput. Phys. Commun.* **59** 399
[18] Perdew J P, Burke K and Ernzerhof M 1996 *Phys. Rev. Lett.* **77** 3865
[19] Lehmann G and Taut M 1971 *Phys. Status Solidi* B **54** 469
Jepsen D and Anderson O K 1971 *Solid State Commun.* **9** 1763
[20] Clerc F, Bovet M, Berger H, Despont L, Koitzsch C, Gallus O, Patthey L, Shi M, Krempasky J, Garnier M G and Aebi P 2004 *J. Phys.: Condens. Matter* **16** 3271
[21] Williams P M and Shepherd R F 1973 *J. Phys.* C **6** L36
[22] Smith N V and Traum M M 1975 *Phys. Rev.* B **11** 2087
[23] Wilson J A, Salvo F J Di and Machajan S 1975 *Adv. Phys.* **24** 117
[24] DiSalvo F J, Schwall R and Geballe T H 1971 *Phys. Rev. Lett.* **27** 310
[25] Beal A R, Hughesi H P and Liang W Y 1975 *J. Phys.* C **8** 4236
[26] Ashcroft N W and Mermin N D 1976 Solid State Physics (New York: Holt Rinehart and Winston Inc) p18